Chapter 3

The preceding chapter described our successful attempt to use momentum-imaging techniques to measure electron spectra. The power of this method becomes evident with the addition of a gas jet as a localized target. In addition to measuring the electron momentum, we can simultaneously measure the momentum of the recoil-ion produced by the same event. Up to this point the recoil-ion measurement has been limited to the determination of the charge-state or ion species. The present chapter will be a description of the addition of a local target to the apparatus, and the use of that target to measure molecular dissociation fragments in addition to the electrons emitted in ion-molecule collisions.

3.1 Molecular Dissociation

When a fast projectile interacts with a molecule, several events can occur which cause the molecule to dissociate in addition to ejecting an electron. These have been the subject of considerable study dating back to 1930 [3.1]. A review of the history and scope of the study of the processes described in this chapter is well documented in "The Dissociative Ionization of Simple Molecules by Fast Ions," by Latimer [3.2]. Possible processes include single ionization, double ionization and ionization-excitation. For

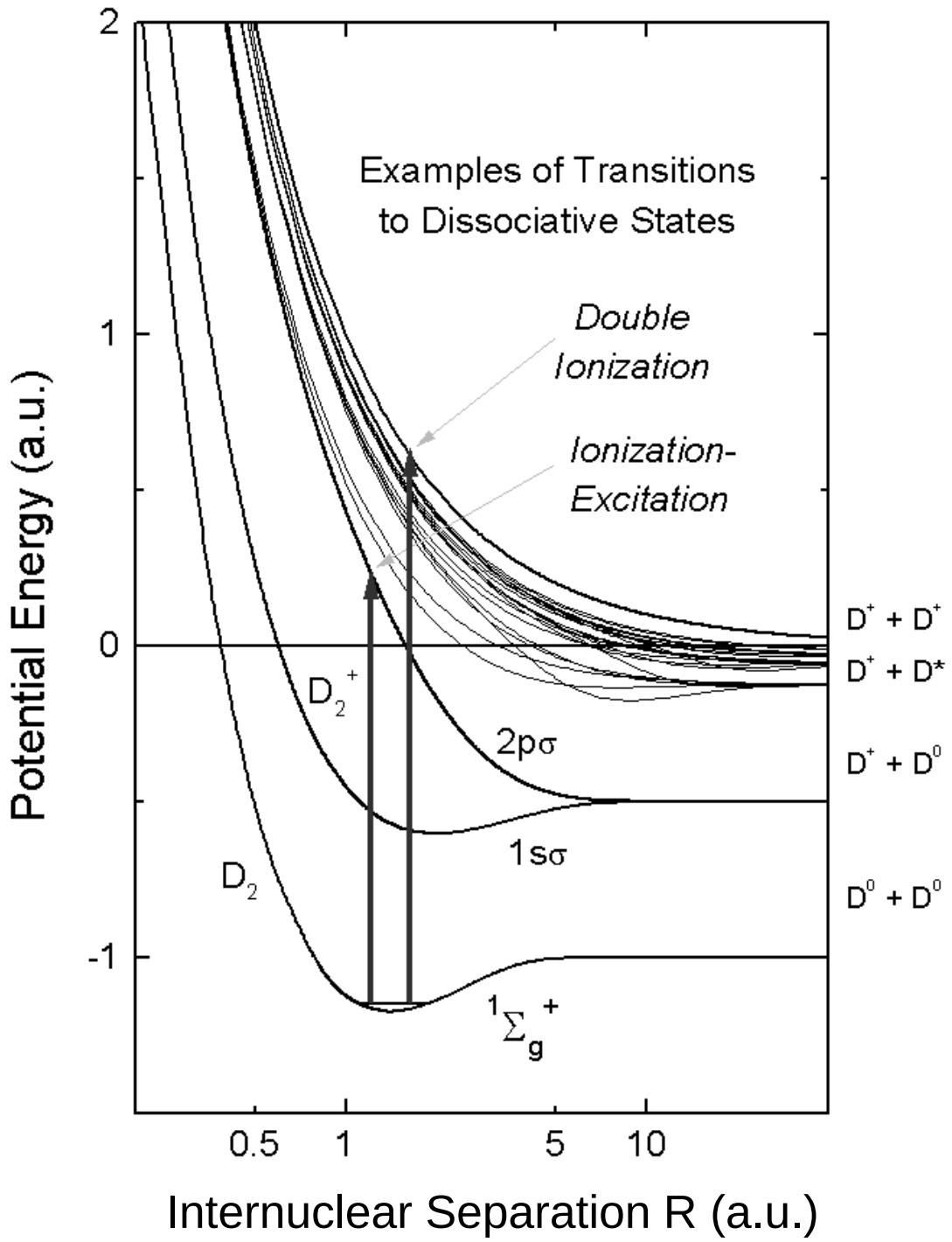

Figure 3.1: Potential curves for neutral, singly and doubly ionized deuterium. The vertical lines represent transitions to dissociative states.

example, if the molecule is singly ionized, then one electron is ejected, and the remaining molecular ion can be in the ground electronic state, or an excited electronic state. These two cases are separated into single ionization and ionization-excitation. Double ionization simply refers to the ejection of two electrons from the molecule.

Figure 3.1 shows some of the potential energy curves for a Deuterium molecule in the neutral ground state, some of the singly ionized states, and the doubly ionized state. During a collision with a fast projectile, electronic transitions from the ground state to these excited states happen on a faster time-scale than the vibrational motion of the molecule. Such vertical (or "Franck-Condon") transitions leave the molecule with the same internuclear separation as it had in its ground state. As can be seen from the figure, all but the ground state of H_2^+ are repulsive, causing the molecule to dissociate with a few electron volts of kinetic energy.

The energy of the remaining fragments is then dependent upon the final state. The dissociation energy is the difference between the potential energy of the state immediately after the vertical transition and the energy of the fragments at infinite internuclear distance. Take two examples. In the simplest case of double ionization, both electrons are quickly ejected, and the kinetic energies of the two bare nuclei in the final state are determined by their mutual Coulomb potential. In the case of a transition to the $2p\sigma$ state, the binding energy of the neutral fragment must be included in this energy difference. In addition, because the molecule has vibrational motion, the initial internuclear separation is not well defined, causing a spread in the corresponding fragment energies.

When the molecular ion dissociates after a collision, the molecule explodes more quickly than it rotates. The explosion time is of the same order as the vibrational period, or on the order of a few femtoseconds. This time is much shorter than the rotational period, which is of the order of hundreds of picoseconds. Therefore, to a very good approximation, the fragments are ejected along the direction of the internuclear axis. Thus, the measurement of the fragment ejection angle is essentially a direct measurement of the spatial alignment and orientation of the molecule immediately prior to the collision.

We will begin by describing the apparatus and technique used for our measurements. We then divide our results into two groups. First, we will discuss dissociation energy and alignment measurements of the molecules. We then report electron measurements correlated to the alignment of the molecule. Within each section, we will compare our data to that of related works.

3.2 Apparatus and Method

Figure 3.5 shows a scale rendering of the apparatus used for the measurement discussed in this chapter. The technique used in this experiment is similar to that described in chapter 2. The major apparatus change is the addition of a gas jet. The gas jet design and operation are detailed in appendix B. Because the jet forms a well defined, localized target, we know in principle the point of origin for all of the particles produced in the ion-molecule collision. This allows us to measure the complete momentum vector of one outgoing deuteron in coincidence with two components of the momentum vector of one ejected electron. We can therefore determine the alignment of the molecule at the

time of the collision and how two components of the electron momentum relate to this alignment.

The other notable difference from the preceding experiment was that the spectrometer was modified to create a symmetric geometry between the electron detector and recoil detector acceleration regions. The maximum breakup energy for a deuterium molecule dissociated through a Frank-Condon transition is 19 eV, or 9.5 eV per fragment. This is of the same order of magnitude as the electron energy range in which we are interested. Because electrostatic analyzers discriminate based upon energy, such a symmetric geometry was a logical choice. By applying fields such that all deuterium fragments landed within the boundaries of the recoil detector, electrons of the same energy range hit the electron detector. As described in chapter 2, we used position and time information to determine the components of the momentum vectors for one deuterium fragment as well as one electron.

One of the drawbacks of such an arrangement is that due to the high field of the spectrometer, TOF_e was too short to measure accurately. At the time of this experiment, we simply used a DC ion beam and did not directly measure TOF_e. We did measure the recoil ion TOF and so were able to obtain the full momentum vector of the molecular fragment and two components of the electron momentum vector. Though not ideal, this proved sufficient to study the correlated electron spectra.

Another difficulty with this particular experiment was the presence of diffuse background deuterium gas, or what we refer to as hot gas, that found its way into the target region. Early versions of the gas jet design allowed for leaks from the nozzle

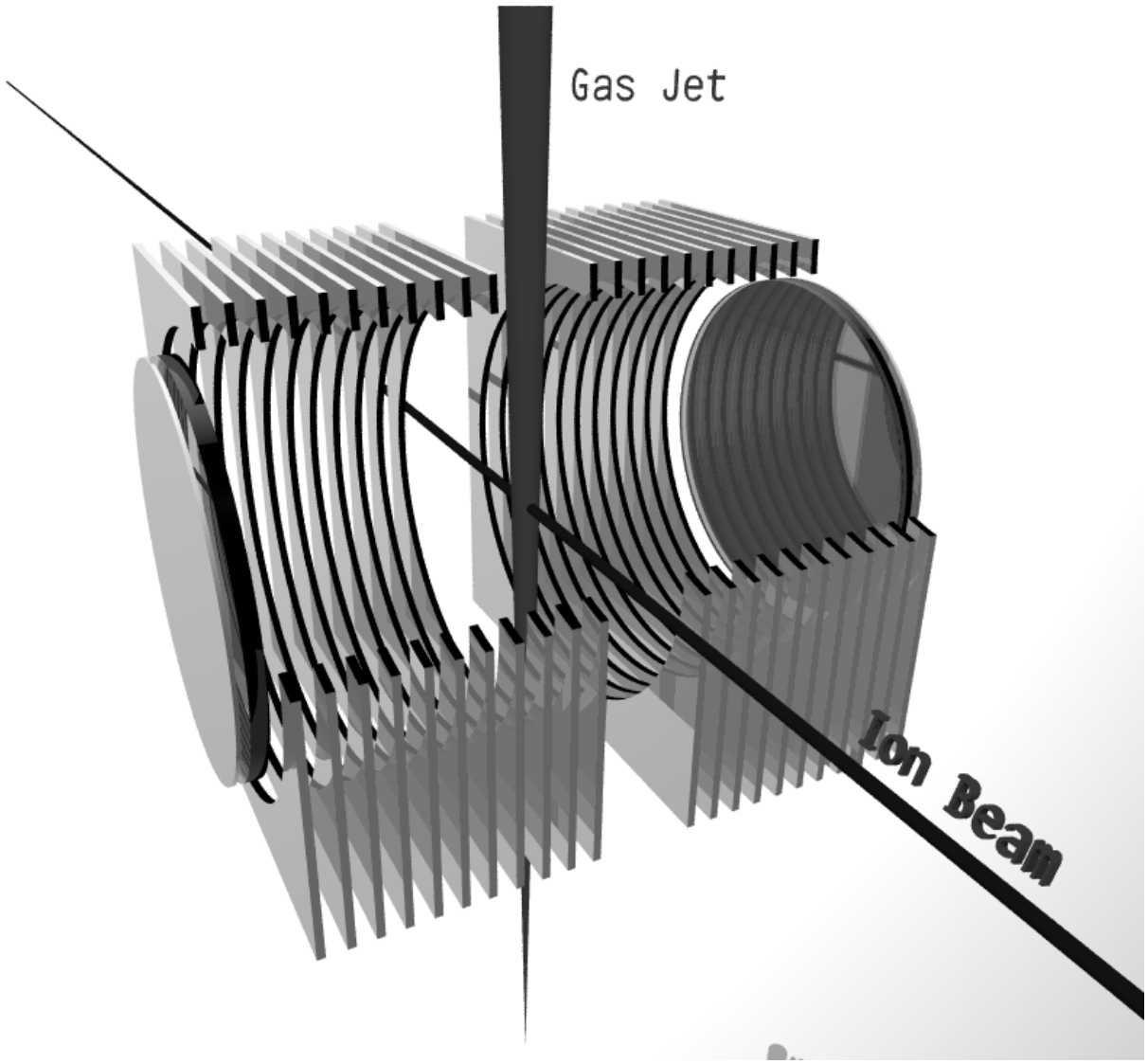

Figure 3.2: Scale rendering of the momentum imaging spectrometer configured for the deuterium experiment. The glass discs at either end of the spectrometer are microchannel plate detectors for the electrons and recoil ions.

vacuum chamber into the target vacuum chamber. Due to the necessary fields and design required to capture the molecule fragments on the detector, any warm background gas that was ionized by the beam was extracted to hit the detector as well. In order to correct for this, we introduced deuterium gas into the chamber in such a fashion that the target was not localized, and used data taken in this mode as a background for subtraction. Current gas jet technology has improved, primarily through the use of multiple stages, to a point where this effect has become negligible.

The specific ion beam that we used for this experiment was again 30 MeV bare carbon. One of the difficulties outlined in chapter 2 was still apparent. There was no a priori way to determine the z = 0 position on the electron detector. This system allowed us again use the Tribedi data for this calibration. Because to date there hadn't been any experiment of this type, we felt that this particular system was a convenient choice. We will divide the discussion into two sections, beginning with molecular fragment measurements and followed by correlated electron measurments.

3.3 Molecular Fragments

We first turn our attention to the recoil ions produced in the collision. The detectors used in this experiment were the single-hit wedge-and-strip type. We were only able to measure one of the fragments produced in the collision. This would be the cause for some concern, as in the case of double ionization two fragments will arrive at the detector. From conservation of momentum, both deuterons produced will have equal

momenta, directed away from one another. This implies that along the x-axis (field direction), one ion will have momentum toward the detector while the other will have momentum away from the detector.

Because we can only detect one ion, two things can happen. If we detect the first ion, we can never see the second ion in the TAC spectrum because the time signal stops the TAC. Due to the finite efficiency of the detector (see appendix B), the second ion may or may not detected. In the case that it is, the position spectrum is distorted in such a way that the average of the positions is seen. The other possibility is that we don't detect the first ion (again due efficiency), and only the second ion is detected. If we detect either the first or both fragments, then the event registers in the time spectrum as having momentum toward the detector. On the other hand, if we detect only the second fragment, the event registers as having momentum away from the detector.

Figure 3.7 shows raw slices of the recoil distributions in momentum space. The radial distance of each event corresponds to the magnitude of the recoil momentum (proportional to the square root of the fragment energy). One can see the effect of detected multiple hits by noting the portion of the distribution lying along the negative x-axis, which corresponds to both fragments being detected. This is due to the averaging of the position for the two fragments and the first fragment stopping the TAC. In addition, a faint band of counts lies along the z-axis in the x-z and y-z views. This is due in part to unsubtracted hot gas and random events from background gas. Although these effects were accounted for, normalization of the hot gas and random events was problematic.

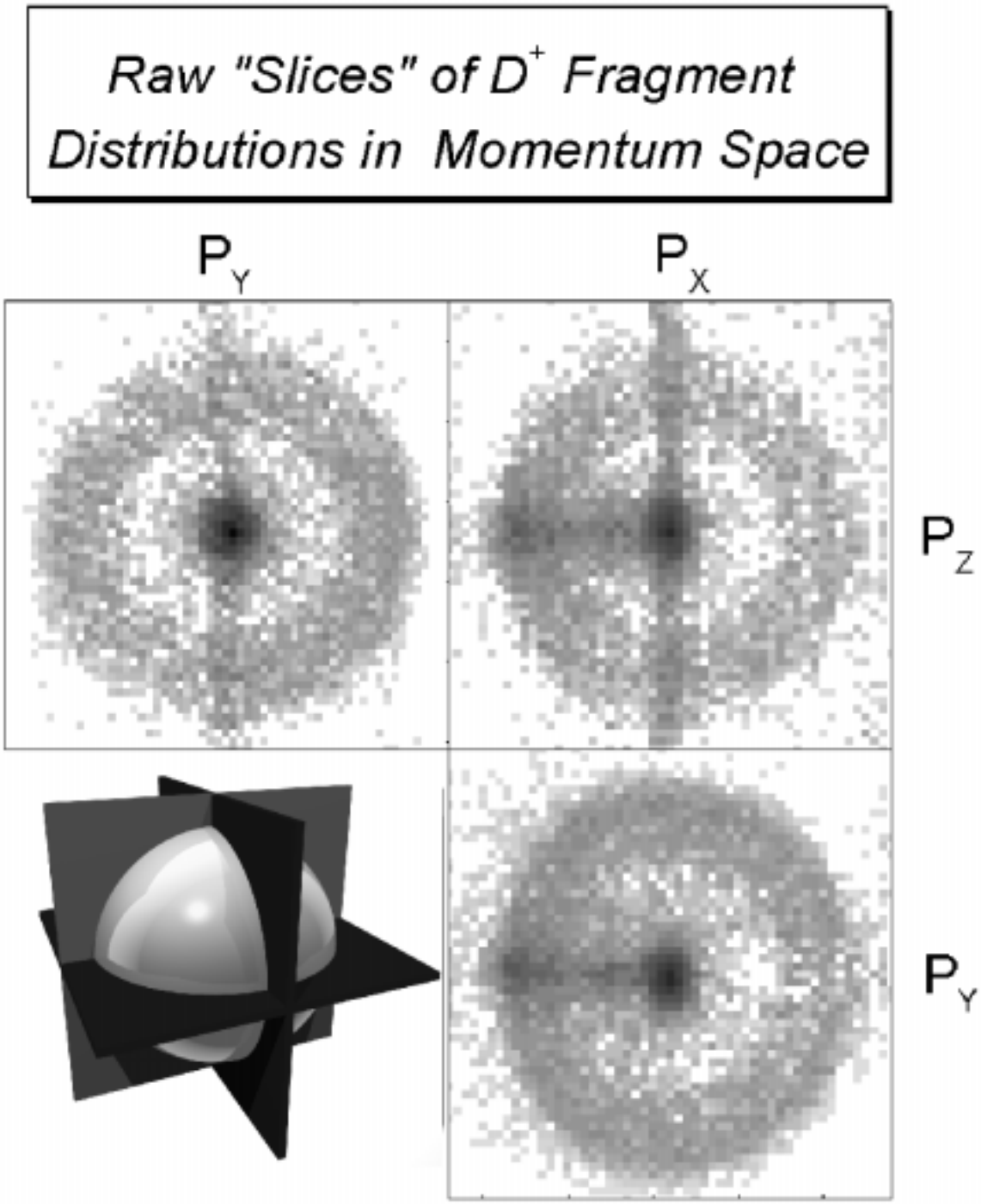

Figure 3.3: Raw momentum spectra of deuterium fragments. The picture at the lower-left illustrates how slices are taken of the sphere formed by the data in momentum space. Note the double-hits lying along the negative portion of the x-axis.

3.3.1 Dissociation Energies

Fragment energy distributions have been measured for some collision systems to a higher degree of precision than the work presented in this dissertation. A good example is the work presented by Edwards *et al* in 1990 [3.2]. They used electrostatic analyzers to measure the molecule fragments produced in dissociative collisions between 0.5 MeV/u protons and molecular hydrogen. Their results are shown in Figure 3.4. Also shown are contributions of various final states of the molecular ion H_2^+ and the doubly ionized state. Each state weighted with a least-square fit of the data to form the resulting solid curve. Included states are the ground state dissociation ($1s\sigma_g$), ionization-excitation ($2p\pi_u$. $2s\sigma_u$, and $2p\sigma_u$), autoionizing states (AI), and double-ionization (H^+H^+).

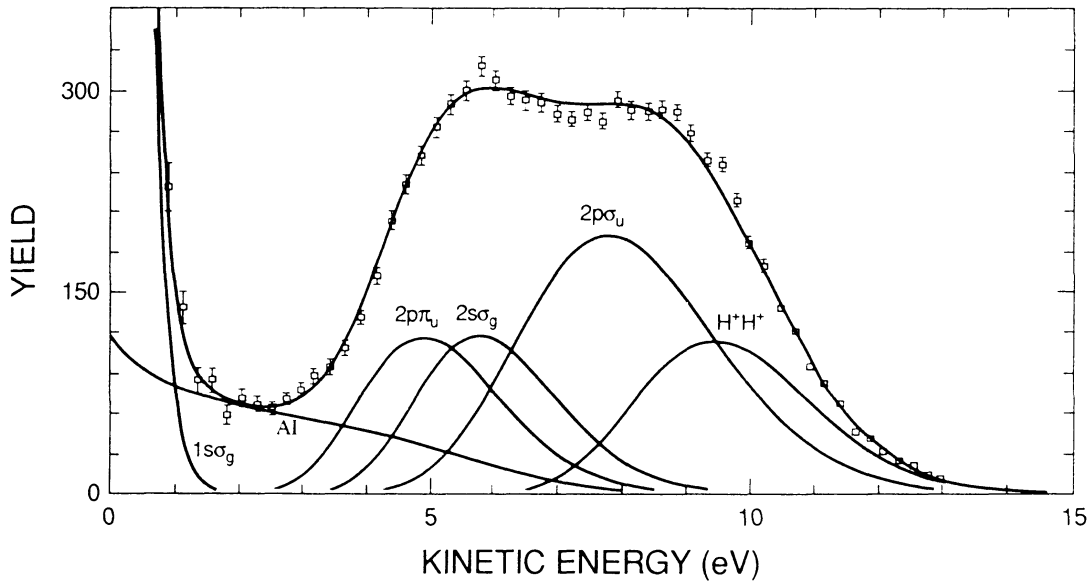

Figure 3.4: Fragment energy distribution for 500keV H^+ + H_2 by Edwards *et al* [3.2]. Note the variety of states that can produce a free deuteron in an ion-deuterium collision.

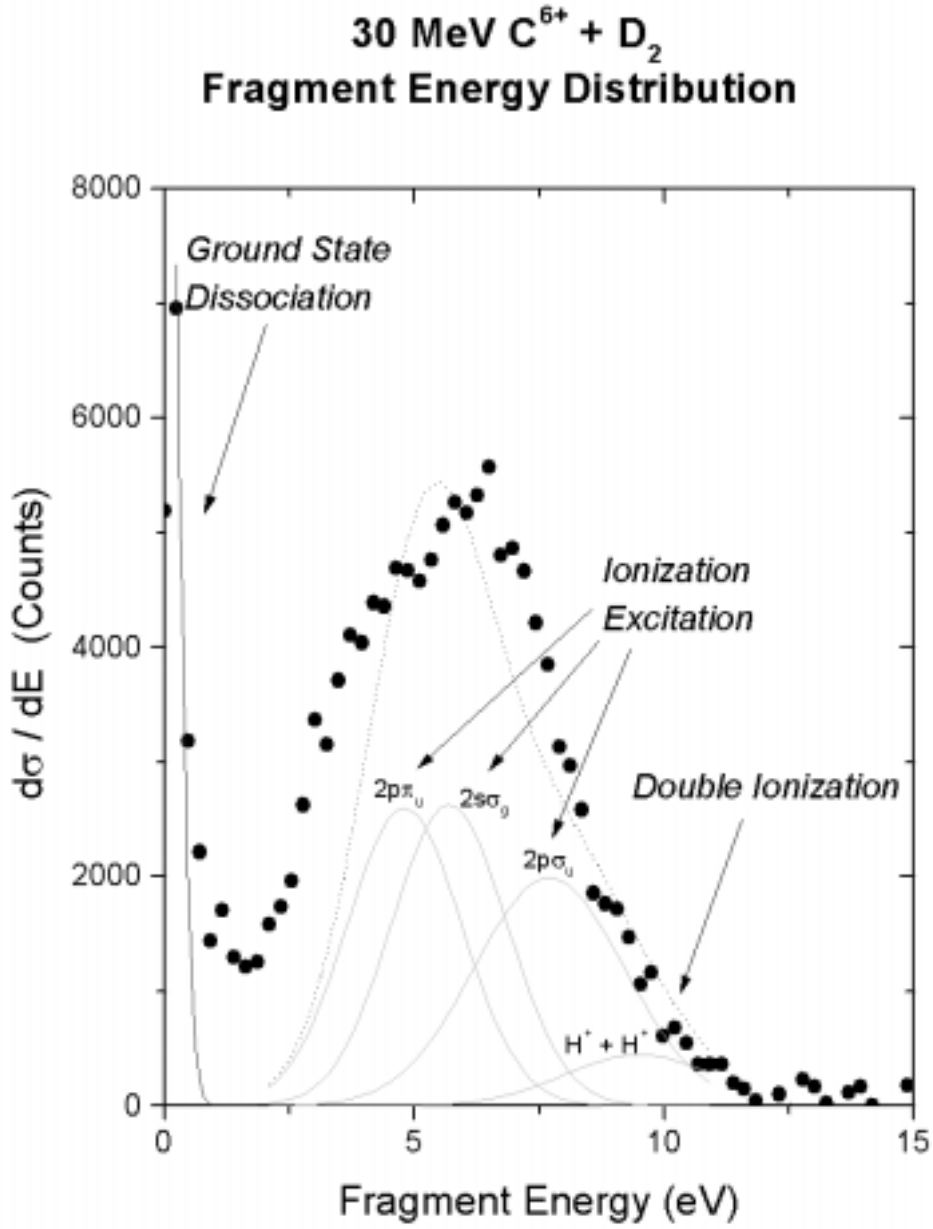

Figure 3.5: Energy distribution of the detected deuterons. This spectrum is obtained by integrating the momentum sphere over all angles pointing away from the recoil detector. Shown is a fit of Guassian distributions for dissociative states.

Figure 3.5 is a similar plot of our radial distribution converted to energy. We have fit our data with the same ionization-excitation and double-ionization curves as used in figure 3.4. Although the focus of this experiment was not to measure the fragment energy distribution, general features in the spectrum can easily be identified. We see the narrow peak at zero energy corresponding to ground state dissociation. In this case, the molecule is singly ionized and promoted to a continuum vibrational state of D_2^+. Due to the evidence of multiple hits, we know double ionization contributes to the fragment production, but from the figure we see that ionization-excitation is clearly the dominant channel.

3.3.2 Molecule Alignment

The relative probability for detecting a deuteron for a given alignment is shown in figure 3.6. In our particular case, as can be seen from figure 3.5, the majority of these deuterons are produced by ionization excitation or double ionization. Both of these processes involve each of the two electrons on the deuterium molecule. As can be seen in the figure, there is a marked minimum in the distribution around 90º, which corresponds to perpendicular alignment. The counts increase at either end of the spectrum corresponding to parallel alignment. This is also predicted by the theory. One explanation of this effect may be that it is more likely for the ion beam to interact with both electrons in the case of parallel alignment of the molecule, and the energetic dissociative states require a two electron transition. Due to the speed of the incoming projectile, we would not expect any distinction in the distribution between the 0º and

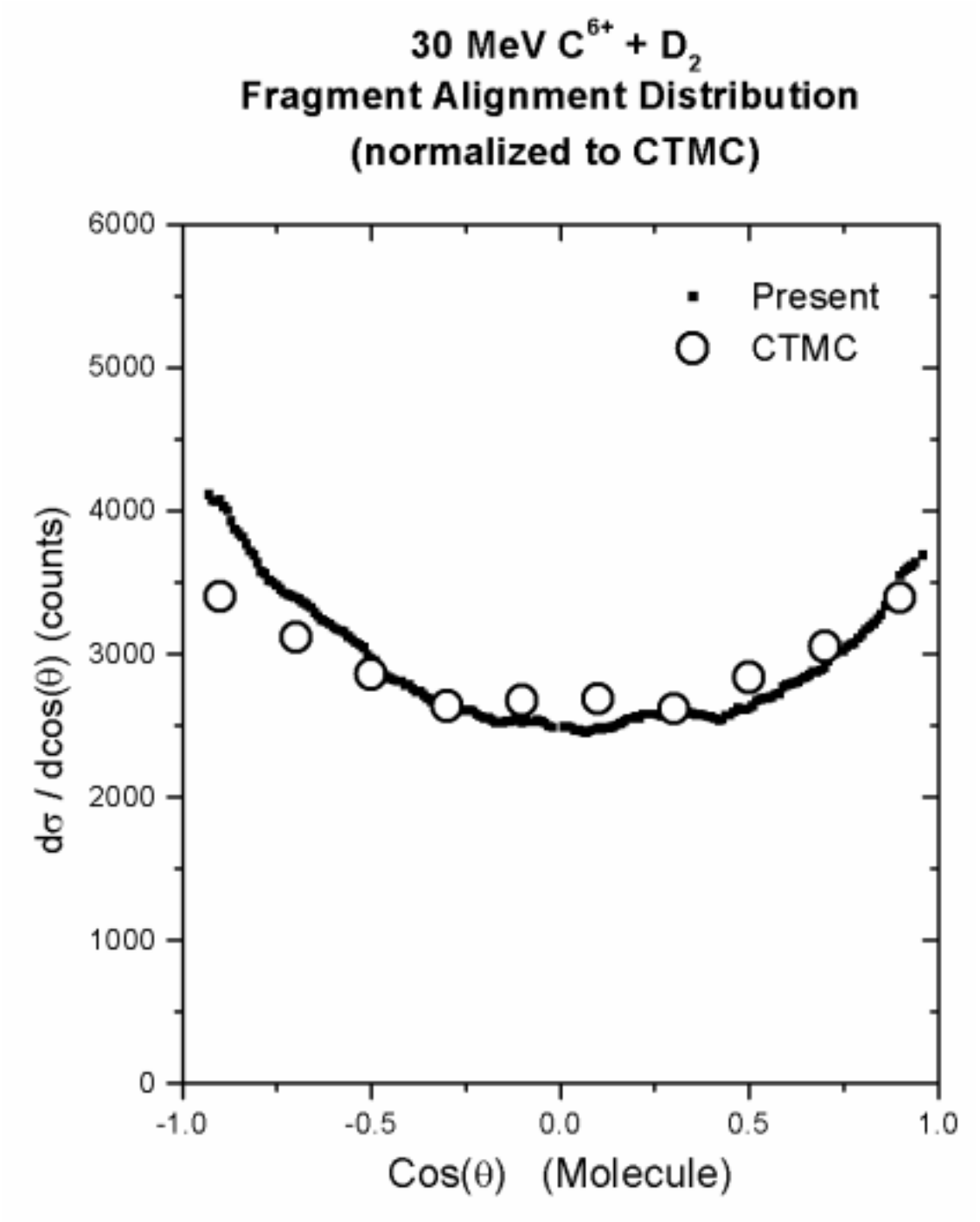

Figure 3.6: Deuterium fragment angular distribution. Also shown is the CTMC calculation by Olson. Our data were scaled to the theory.

180º case. Any asymmetry in the data is due to experimental artifact, in particular the proper choice of the zero z-position on the recoil detector.

3.4 Correlated Electron Momentum Measurements

The major purpose of this section is to report the measured effect of the spatial alignment of the D_2 molecules on the electron momentum distribution. Due to the high fields required to collect the deuteron fragments, we were unable to measure the electron time of flight. We were, however, able to measure their final position on the detector. This is, to a good approximation, directly proportional to the electron momentum in z- and y- directions. Shown in figure 3.7 are density plots of the electron position/momentum for molecules aligned parallel and perpendicular to the beam. In both cases, the molecule was gated to lie parallel to the face of the detector.

Parallel or perpendicular alignments were assigned for molecules whose fragment momenta fell within cones defined by measuring θ_y and θ_z relative to their respective axes. For parallel or longitudinal alignment, we required $|\cos\theta_z| < 0.5$, while perpendicular alignment was defined as $|\cos\theta_y| < 0.5$. This created a cone of ±30º about either axis. In addition, as in the case of all data presented in this experiment, we only accepted recoil ions going away from the recoil detector in order to avoid contamination from multiple hits.

The density plots are simply electron detector images for the parallel and perpendicular orientations of the molecule. Because density plots lack an easily viewed

comparison of the relative intensities, we needed a quantitative presentation of the data. Therefore, we converted these density plots into a polar representation. In order to accomplish this, we had to determine the zero momentum of the electron distribution.

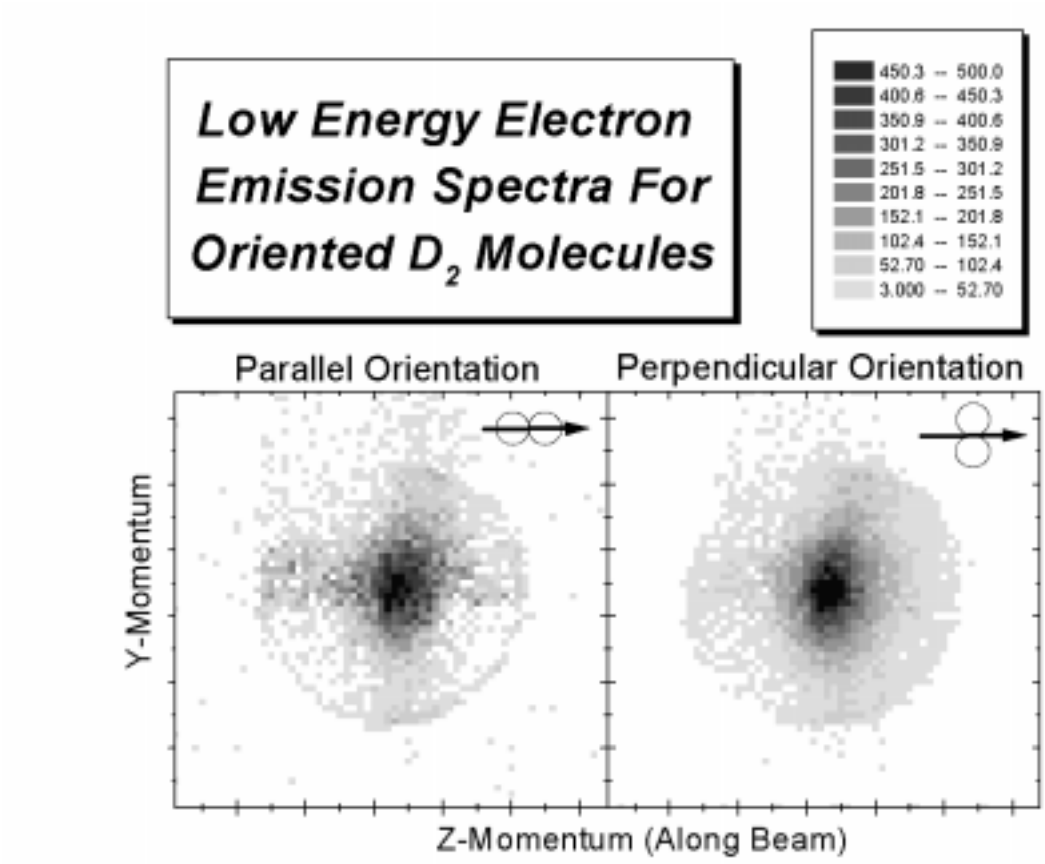

Figure 3.7: Two-dimensional electron distribution for spatially aligned deuterium. The distribution for the parallel molecule appears to be rounder than that for the perpendicularly oriented molecule.

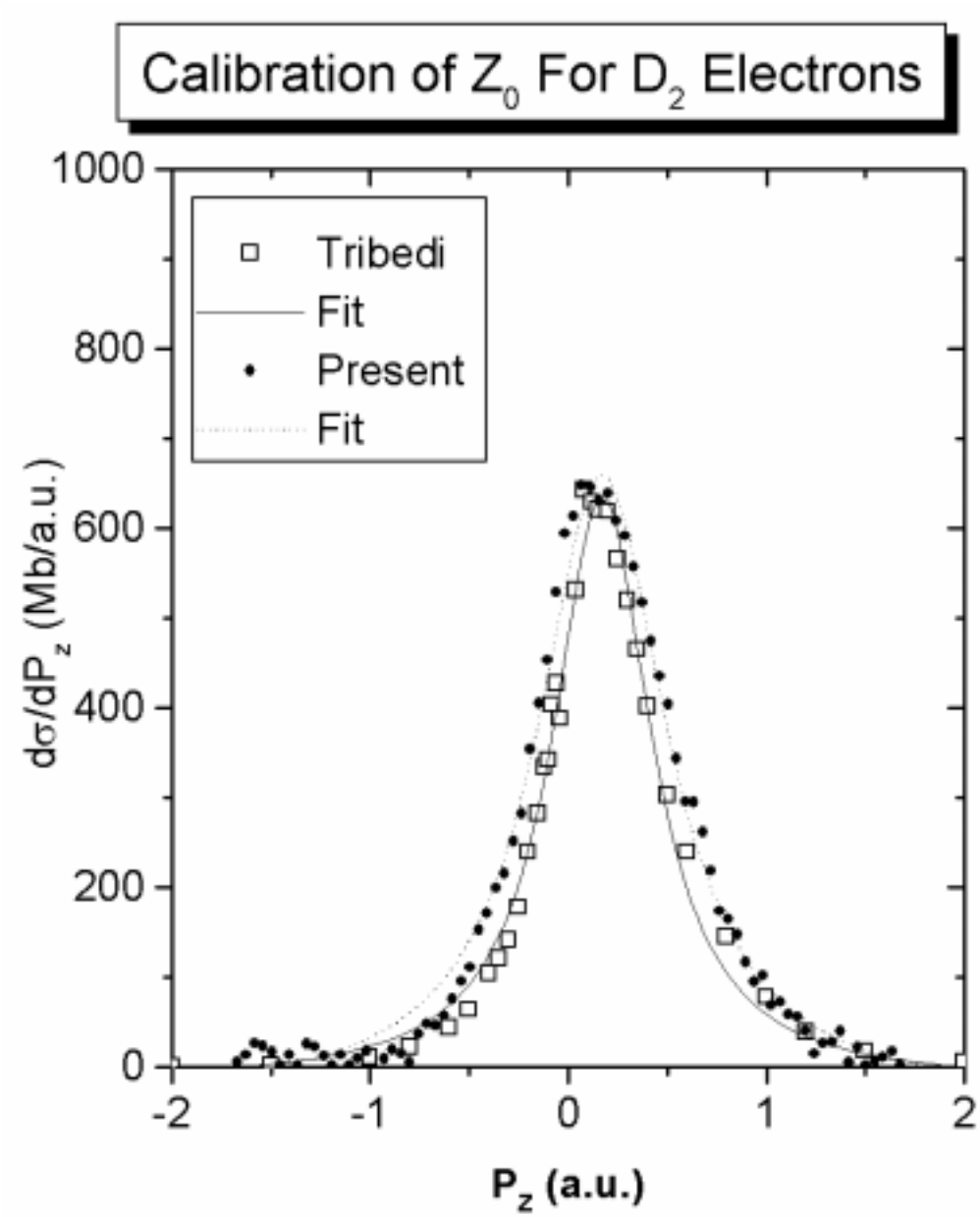

Figure 3.8: Longitudinal momentum distributions used for calibrating the z-position zero. A fit was done to each distribution and then the centroid of our data was shifted to match that of Tribedi.

As described in chapter 2, we had no direct way of measuring the zero position of the electron detector. We were able to determine the zero y-position from symmetry of the electron distribution. For the zero z-position determination, we were again required to use the data of Tribedi [2.2]. The calibration is shown in figure 3.8. In order to get as accurate a zero as possible, functions were fit to both curves, and the centroid of our datawas shifted to match that of Tribedi. Again the deuterium/hydrogen results agree quite well, as in chapter 2. Because in this case the gas jet provides a local target, we used the absolute position on the electron detector for the longitudinal momentum measurement, instead of a measurement relative to the recoil detector position. The width in the distribution can be accounted for by the spatial width of the target gas jet.

In order to convert from position to momentum, we did first-principles calculations of the electron TOF, assuming it had zero momentum toward or away from the detector. For the present data, a value of 4.49 nsec was used. From the resulting transverse distribution, we could see that the momentum value at half-maximum was roughly ±0.5 a.u. By assuming the electron had this momentum toward or away from the detector, we calculated the resultant error in the TOF to be -0.26/+0.29 nsec, leading to an acceptable -5.6%/+6.5% margin of error in the momentum calculation.

Shown in figure 3.9 is the conversion of the data by Tribedi to the polar representation. Although the collision systems measured are essentially the same, as deuterium and hydrogen are chemically equivalent targets, there are definite distinctions between the two experiments aside from the technique. For the present experiment, our data were restricted to only coincidences with a fragment of the molecule, while the data

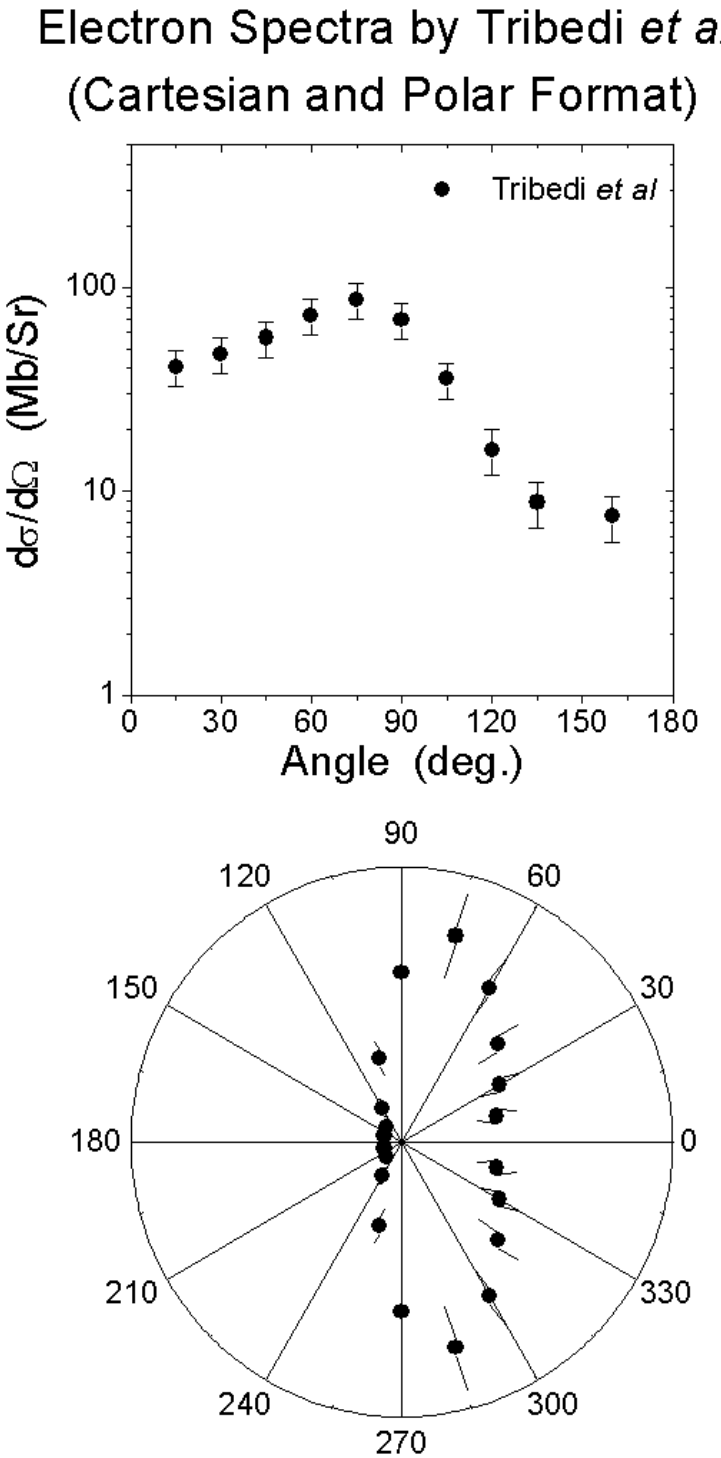

Figure 3.9: Electron angular distributions for 30 MeV C^{6+} as measured by Tribedi presented in histogram and polar format.

of Tribedi included all ejected electrons. In addition, as described before, we had to integrate over the x-momentum component of the electron distribution. Therefore our angle calculation only included the z- and y-components. However, some similarity can be seen between the data of Tribedi, and our results shown in figure 3.10.

We have converted the data shown in figure 3.7 to a polar representation. Shown in figure 3.10 are the spectra for electron production corresponding to particular molecule alignments. The data are binned according to the magnitude of their individual momentum (again, integrating over P_x). The angle relative to the z-axis was calculated, and then the data were mirrored for presentation. We have normalized the parallel and perpendicular spectra so that for the data shown, the total integrated counts are equal. The radius of each plot is 2000 counts. We were wary of any conclusions about the data along the z-axis, or from 175˚ to 195˚ and from 345˚ to 15˚. It is in this region that the hot gas contamination is most prevalent, and the subtraction most difficult. Therefore, that data was omitted. There is no reason to consider data outside these boundaries suspect.

One can clearly see a progression from isotropic distributions at low electron energy to a marked transverse distribution at higher electron energies. We speculate that this trend is in part due to the change in the mechanism of electron production from soft three-body type collisions to a hard two-body type collision. The latter should produce more energetic electrons, and for the regime in which we measure they should lie transverse to the beam. This corresponds to the low energy portion of the binary encounter ridge defined by the kinematics of the two-body ion-electron collision. There

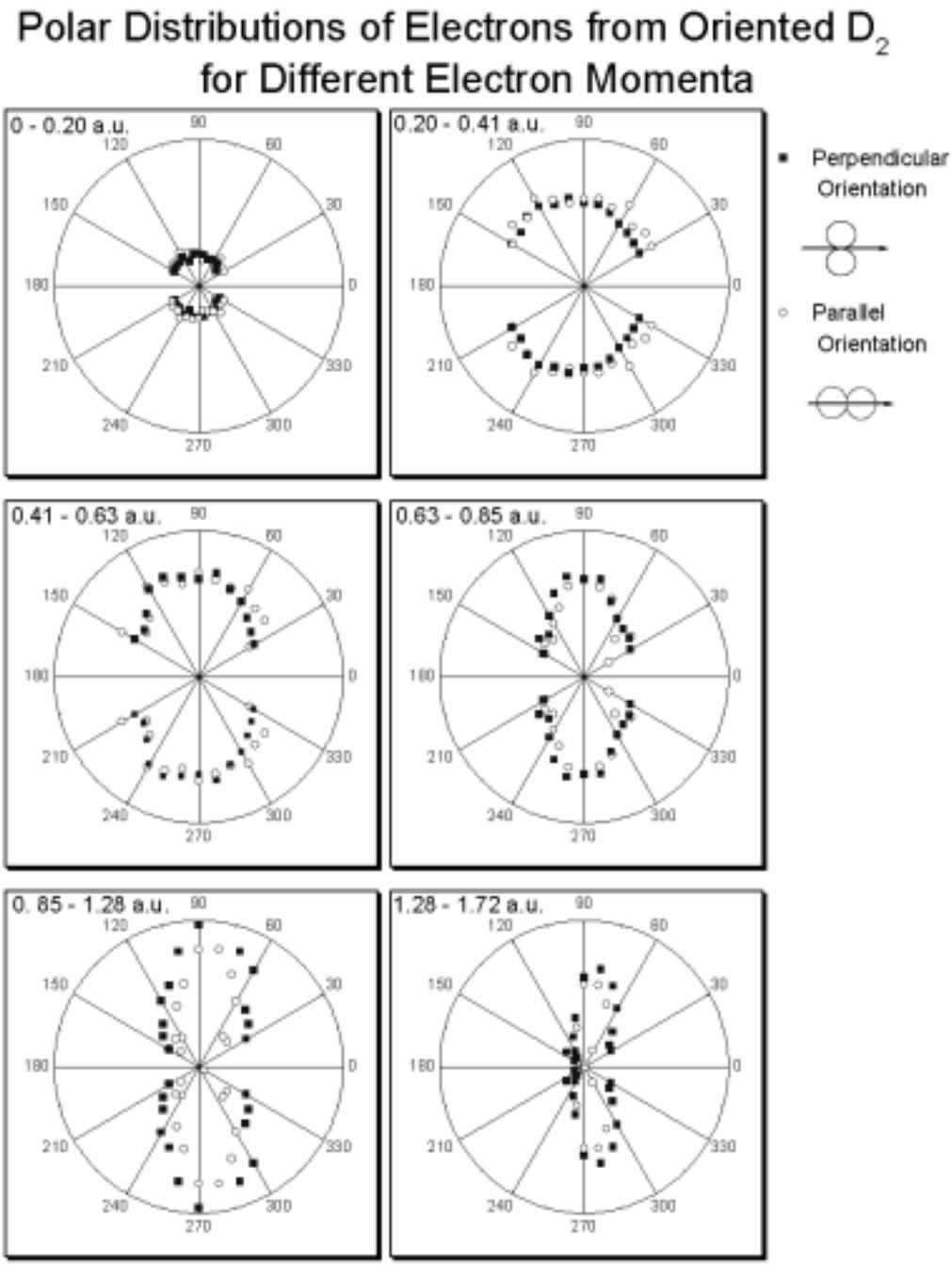

Figure 3.10: Polar plots of ejectred electron momentum for parallel and perpendicular molecule alignment. Because of the necessary integration over momenta perpendicular to the detector, the angle is always measured in the detector plane. (The Tribedi data are distributions of "true" cylindrical coordinate θ_e). The plots are binned for varying magnitudes of electron momentum (again in the detector plane).

is a strong similarity to the higher energy electron spectra and the polar plot representation of the Tribedi data. Furthermore, there is an enhanced transverse momentum distribution for electrons ejected from molecules aligned perpendicular to the beam.

Very few correlated measurements of electron spectra and molecular fragments exist in the literature. One example that is very closely related is the measurement of double photoionization of spatially aligned D_2 by Dörner [3.4]. Using momentum-imaging techniques similar to ours, they measured solely the double ionization reaction channel. With state-of-the-art multi-hit detectors and a two stage gas jet, they were able to measure in coincidence both outgoing deuterons and one of the ejected electrons. The correlated electron momentum for the Dorner experiment can be seen in figure 3.11. The anisotropy of the distribution is not only dependent upon the molecular alignment, it is also affected by the polarization of the light. One general trend however, is that the electrons seem to be preferentially ejected along the polarization vector, a feature which is enhanced when the molecule lies along that same axis. In our measurement, the convenient axis of reference is the beam, and it is important to note that the time-averaged electric field produced in the fast ion-molecule collision is perpendicular to the beam direction.

From these data, we draw two conclusions. In both cases of ionization by photons and ionization by ions, the ejected electrons are distributed along the ionizing field vector in momentum space. Furthermore, this effect is enhanced when the molecule lies along that same axis.

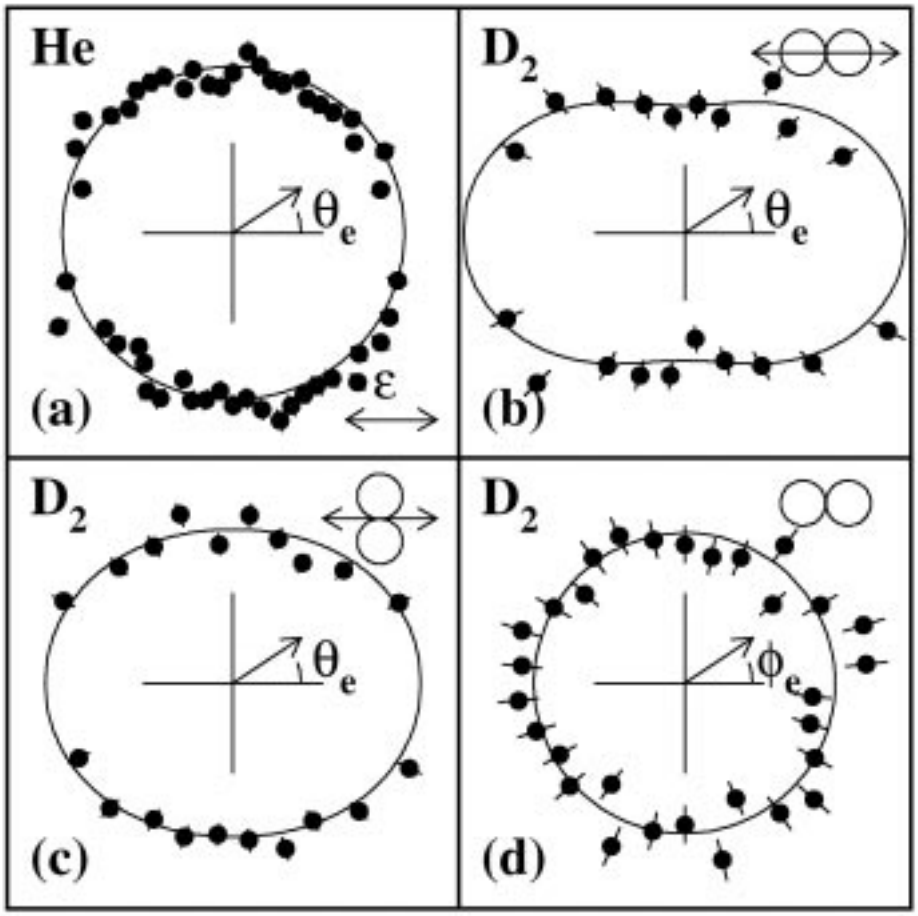

Figure 3.11: (Data of Dörner [3.4]) Polar representation of the angular distribution of one of the two photoelectrons from double photoionization of helium at 7 eV excess energy and of D_2 also at about 7 eV excess. The data have been integrated over all electron energies. (a) $d\sigma/d\cos\theta_e$ for helium with ε along the horizontal. The line shows a fit with $\beta_e = 0 \pm 0.04$. (b) $d\sigma/d\cos\theta_e$ for D_2 with ε along the horizontal and the molecular axis held fixed parallel to ε. The line shows a fit with $\beta_e = 0.4 \pm 0.1$. (c) Similar to (b) but for alignment of the molecule perpendicular to ε. The data are integrated over all azimuthal angles. The line shows a fit with $\beta_e = 0.14 \pm 0.08$. (d) $d\sigma/d\varphi_e$ for D_2 with $70^o < \theta_e < 110^o$ (90° is the plane of the paper). The molecule is held fixed perpendicular to ε, which now points out of the paper. The full line is a circle to guide the eye.